Journal of Magnetism and Magnetic Materials 377 (2015) 44–51

Contents lists available at ScienceDirect

Journal of Magnetism and Magnetic Materials

journal homepage: www.elsevier.com/locate/jmmm

Size and surface effects in the magnetic order of $CoFe_2O_4$ nanoparticles

Betiana N. Pianciola [a,b], Enio Lima Jr.[b], Horacio E. Troiani [a,b], Luiz C.C.M. Nagamine [c], R. Cohen [c], Roberto D. Zysler [a,b,*]

[a] Instituto Balseiro, S.C. Bariloche 8400, Argentina
[b] Centro Atómico Bariloche – CNEA/ CONICET, S.C. Bariloche 8400, Argentina
[c] Instituto de Física, Universidade de São Paulo, São Paulo 05508-090, Brazil

ARTICLE INFO

Article history:
Received 19 June 2014
Received in revised form
14 October 2014
Available online

Keywords:
Fine particles
Superparamagnetism
Magnetic ordering
Size effects
Surface effects

ABSTRACT

In this work, we have focused on the size dependence of the magnetic properties and the surface effects of $CoFe_2O_4$ nanoparticles synthesized by high-temperature chemical method with diameter $d \sim 2$, 4.5, and 7 nm, with narrow size distribution. transmission electron microscopy (TEM) images and X-ray diffraction (XRD) profiles indicates that samples with 7 and 4.5 nm present a high crystallinity while the 2 nm sample has a poor one. We have investigated by magnetization measurements and in-field Mössbauer spectroscopy the influence of the surface in the internal magnetic order of the particles. Particles with $d=7$ nm have almost single domain behavior and the monodomain occupies approximately the whole particle. In the sample with $d=4.5$ nm the surface anisotropy is large enough to alter the ferrimagnetic order in the particle shell. Then, a surface/volume ratio of $\sim 60\%$ is the crossover between a single domain nanoparticle and a frustrated order in a magnetic core–shell structure, due to the competition between surface anisotropy and exchange interaction+crystalline anisotropy in cobalt ferrite. In the $d=2$ nm sample the poor crystallinity and the large surface/volume ratio avoid the ferrimagnetic order in the particle down to $T=5$ K.

1. Introduction

Surface and finite size effects in very fine (< 7 nm) magnetic nanoparticles have been the subject of growing interest in recent years from both, theoretical and experimental, points of view [1–3], since they could be definitively used for the technological application of these systems. Finite-size effects dominate the magnetic properties of nanosized particles and become increasingly important as the particle size decreases, due to the increasing surface-to-volume ratio. The magnetic properties of a perfectly aligned single-domain particle where all spins fluctuate coherently are not observed for system where the number of misaligned spins on the surface is a significant contribution. It is expected that the decrease in the coordination number induces a weakening in the exchange interactions of the surface atoms with the surrounding ones. Such spin disorder propagates from the surface to the core. There are indications of very complicated spin structures for nanoparticles with reduced size as consequence of the competition between the surface anisotropy and exchange energy plus magnetocrystalline anisotropy.

It is well established that in small size particles, the surface spins play a dominant role. These spins cause the reduction in saturation magnetization and coercivity with decreasing particle size at the nanometric range [4]. It has been shown that in ferrite nanoparticles, due to the broken symmetry and exchange bonds at the surface, the surface spins do not follow the core anisotropy direction and become disordered or canted, leading to even higher anisotropy compared to the nanoparticle core [1,5–8]. Such particles have a core–shell structure, where the core spins are magnetically ordered, and the shell is composed of disordered or canted spins. Several nanocrystals present the magnetic core–shell structure such as: nickel ferrite [1], NiO [9], Mn_2O_3 [10], Fe_3O_4 [7,11,12], and also in amorphous nanoparticles [13] where a spin canting at the surface exist. In these cases, the observed magnetic behavior is explained with a model where the canted spins are in a surface layer and they freeze into a spin-glass-like phase at low temperatures. As a consequence, the surface spins have multiple configurations for any orientation of the core magnetization.

An interesting system to study this phenomenon is the cobalt ferrite ($CoFe_2O_4$). The material in bulk has well known nature, and because of the high crystalline anisotropy has also been intensively studied because of their possible use in technological applications. Moreover, the local surface anisotropy due to the iron and cobalt ions have easy axes with different directions which favor the magnetic disorder canting of the spins at the surface.

* Corresponding author at: Centro Atómico Bariloche – CNEA/ CONICET, S.C. Bariloche 8400, Argentina. Fax: +54 294 4445299.
E-mail address: zysler@cab.cnea.gov.ar (R.D. Zysler).

http://dx.doi.org/10.1016/j.jmmm.2014.10.054
0304-8853/

Furthermore, it is possible to synthesize ferrite nanoparticles with size control and high crystallinity. In particular, with the decomposition of organometallic precursors (transition metal acetylacetonate) nanoparticles have been fabricated in a one step process, controlling the size in the 2–25 nm range with a narrow size distribution [11,14]. Many papers referring size effects on $CoFe_2O_4$ nanoparticles can be found in the literature [15–18], but non of them study these effects for particles less than 5 nm, where the surface effects are absolutely dominant.

In this work, we have focused on the size dependence of the magnetic properties and the surface effects of $CoFe_2O_4$ nanoparticles synthesized by high-temperature chemical method with $d \sim 2.0$, 4.5, and 7.0 nm, with narrow size distribution. As-made nanoparticles are covered by a monolayer of oleic acid strongly linked to the surface. According to our magnetization measurements as function of field and temperature ($M(H,T)$), as well in-field (up to 12 T) Mössbauer spectroscopy (MS) results, our systems present strong differences between the behavior of the larger-nanoparticles (with high ferrimagnetic order degree) and the smaller-nanoparticles, which present a core–shell magnetic structure, with a magnetically ordered core and a magnetically disordered shell.

2. Experimental details

Nanoparticles narrow diameter distribution were prepared by the high-temperature decomposition of $Co(acac)_2$ and $Fe(acac)_3$ with the 1:2 M ratio (0.6:1.2 mmol) together with 1–2 octanediol, diphenyl ether (boiling point at ~550 K) and oleic acid and oleylamina as surfactants. The particle size was tailored by the surfactant:precursor molar ratio ([Surf.]:[Prec.]) according to the reference [15]. The preparation was magnetically stirred and heated up to the boiling temperature $T \sim 535$ K for 120 min. After synthesis the nanoparticles were extracted by adding ethanol followed by centrifugation (14,000 rpm/30 min). After that, they were washed with acetone and centrifuged once again. The final sample consists in a black powder constituted by cobalt ferrite nanoparticles covered with an oleic acid layer, which is strongly linked to the surface, improving the chemical stability, and avoiding agglomeration. The samples were labeled S2, S5, and S7 with mean diameter 2.0, 4.5, and 7.0 nm respectively, obtained from the TEM analysis.

TEM and high-resolution microscopy (HRTEM) images were made in a Philips CM200 (200 kV) transmission electron microscope. The samples were prepared by dropping a colloidal solution of nanoparticles onto a carbon-coated copper grid. XRD patterns were collected in θ–2θ geometry with a Philips W1700 diffractometer, using Cu-Kα radiation.

In order to avoid dipolar interactions among the particles in the magnetic measurements, the nanoparticles were dispersed in a polymeric matrix (polyethylamine – PEI) in a concentration of ~1% w/w. $M(T)$ in zero-field-cooling (ZFC) and field-cooling (FC) conditions and M(H) loops at $T \geq 2$ K were measured in a commercial SQUID magnetometer.

In-field MS were taken at 4.2 K in a liquid He flow cryostat with a spectrometer in transmission geometry using a ^{57}Co/Rh source. Mössbauer samples were prepared by dispersing 20 mg of the respective powder samples in boron nitride and pressing it between acrylic disks. The sample was mounted in the bore of a 140 kOe superconducting magnet, in a vertical source-sample-detector setup such that the direction of gamma-ray is parallel to the direction of applied field. A sine-shaped velocity waveform was used to minimize mechanical noise. All MS spectra were fitted by using Lorentzian line shapes with a non-linear least-square program (NORMOS), calibrating the velocity scale with a α-Fe foil at 300 K. When necessary a hyperfine field distribution was employed. Isomer shift (IS) values are relative to α-Fe at 300 K. As a consequence of the experimental setup, the temperature of the source during the low temperature spectrum acquisition must to be considered as an important factor to the IS values observed in order to compare with the expected ones.

3. Results

The XRD patterns of the samples S2, S5, and S7 are shown in Fig. 1. The peaks in the patterns of samples S7 and S5 correspond to the expected inverse spinel structure of $CoFe_2O_4$ (PDF 00-022-1086), while sample S2 exhibits a poor crystallinity and only a broad peak associated to the plane (311). There is a broad maximum in the XRD pattern of the samples, which is strong for sample S2, notable for sample S5 and almost imperceptible for sample S7. This broad maximum is resulting from the organic phase remnant from the washing procedure; because its reduced diameter, the washing procedure was more difficult in sample S2. The crystallite mean size was obtained from the peak (311) for the three samples by the Scherrer's equation [19], obtaining 1.6, 4.2 and 7.5 nm, respectively.

Fig. 2 shows the typical TEM images of the as-prepared nanoparticles. The particles appear separated from each other without agglomeration. From several images of different zones of the sample, the diameter histogram of each sample was determined (see Fig. 2b). For all samples, the histogram is well fitted with a lognormal distribution giving mean diameters of $<d>=2.0$, 4.5, and 7.0 nm for samples S2, S5, and S7, respectively. A narrow size distribution was found for all samples ($\sigma=0.1$–0.2). These nanoparticle sizes give a surface/volume ratio (considering a 0.6 nm surface layer, which is close to the first atomic layer distance in lattice) of 0.80, 0.60, and 0.45, respectively. Comparing with the crystallite size obtained from XRD profiles, the diameter of sample S7 is slightly smaller, while for sample S2 and S5 it is slightly larger. HRTEM images show high crystallinity of S5 and S7 samples and poor crystallinity in the S2 sample. A detail of the crystalline planes for sample S7 is showed in the respective bottom panel inset.

Fig. 3a shows the results of $M(T)$ ($H=50$ Oe) as a function of temperature for the S7, S5, and S2 samples are reported. The measurements were performed according to the usual ZFC and FC procedures. S5 and S7 samples present similar curves, typical for single domains of non-interacting systems where the ZFC and FC magnetization curves superimpose at high temperatures (superparamagnetic regime) and, below the irreversibility temperature (T_{irr}), the ZFC magnetization presents a maximum whereas the FC magnetization curve increases monotonically with decreasing the temperature. T_{irr} corresponds to the highest blocking temperature, i.e. to that of particles with highest energy barrier. For the S5 sample, the FC magnetization curve change the slope at $T \sim 50$ K and remains quasi constant at lower temperatures. The shift in the T_{irr} values, $T_{irr}(S7)=300$ K and $T_{irr}(S5)=130$ K is due to the change of the nanoparticle volume, and consequently on the anisotropy energy barrier KV. For weakly interacting nanoparticles the energy barrier distribution, $f(T)$, can be calculated from the $M_{ZFC}(T)$ and $M_{FC}(T)$ curves [20,21]:

$$f(T) \propto \frac{1}{T}\frac{d}{dT}[M_{ZFC}(T) - M_{FC}(T)] \quad (1)$$

This $f(T)$ function presents a maximum at certain temperature that corresponds to the blocking temperature (T_B) of the particles with size of the mean value of the distribution. Fig. 3b shows the energy barrier distribution obtained by the differentiation of the $M_{ZFC}(T)$–$M_{FC}(T)$ curves and divided by T of the samples S5 and S7.

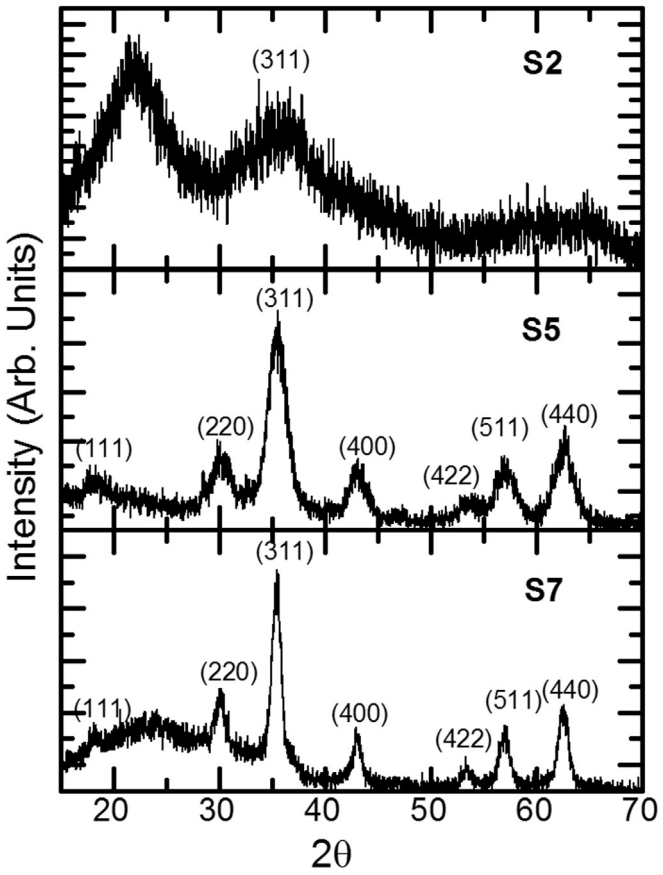

Fig. 1. X-ray diffraction (XRD) profiles of as-made samples S2, S5 and S7.

The $f(T)$ has the same shape (lognormal distribution) as the volume distribution obtained by TEM measurements. Sample S7 distribution curve does not follow the lognormal distribution at $T > 230$ K because the system does not allow the total superparamagnetic regime even at room temperature, then contribution of larger nanoparticles is missing distorting the curve at high temperatures (up to 300 K). A more expected behavior is observed for sample S5, with a lognormal distribution of energy barrier with maximum at ~55 K, despite an unexpected and marked increase in the values of $f(T)$ is observed for $T < 5$ K. On the other hand, in the sample S2 the ZFC and FC magnetization curves almost superimpose at all temperature range. The small irreversibility observed is a consequence of some larger nanoparticles which become blocked at ~60 K.

$M(H)$ curves were performed in ZFC condition at different temperatures. Fig. 4 shows representative $M(H)$ curves for the three samples. For samples S5 an S7, above T_{irr} the magnetization curves are reversible, whereas for $T < T_{irr}$ a hysteretic behavior is observed. On the other hand, sample S2 shows only reversible behavior for the entire temperature range. For all samples, $M(H)$ curves do not saturate up to $H = 5$ T, and in Fig. 5a we plot the magnetization values measured at $H = 5$ T as a function of temperature. The $M(H = 5\ \mathrm{T})$ decreases slowly with increasing temperature for S5 and S7 samples, whereas this reduction is stronger for the smaller particles (S2).

In Fig. 5b the coercive field as a function of temperature data $[H_C(T)]$ for S5 and S7 samples is plotted. The $H_C(T)$ values for both samples can be fitted by using the expression $H_C(T) = H_C(0)\,[1 - (T/T_B)^{1/2}]$ (at $T > 5$ K for S5 sample). This function is characteristic for non-interacting single domains. In the S5 sample, for $T < 5$ K display a decrease of the coercivity which may point out an internal process in the magnetic order of the nanoparticles and will be discussed latter.

Fig. 6a and b present the in-field MS at 4.2 K for sample S7 and S5, respectively. For both samples, the spectra were well-fitted considering two sextets referents to the A (tetrahedral) and B (octahedral) sites of the Fe in spinel structure. We have studied detailed the dependence of D_{23} (relation A2/A3, where A3 and A2 are the intensities of the third and second line, respectively) and of effective field (B_{eff}) with applied field (H_{app}). B_{eff} and the hyperfine field (B_{hf}) are related by $\vec{B}_{eff}(H_{app}) = \vec{B}_{hf}(0) + \mu\vec{H}_{app}$, where μ is the particle magnetic moment. Relevant hyperfine parameters obtained from the fitting procedure are given in Table 1. Because of the strong antiferromagnetic exchange coupling, the B_{eff} of crystalline site A increase, while the one of crystalline site B decrease with H_{app} [11].

Fig. 7a shows the in-field MS spectra at 4.2 K with $H_{app} = 0$, 30, 40, 80, 120 kOe for sample S2, while Fig. 7b exhibits the in-field MS of this sample taken with $H_{app} = 12$ kOe and temperature of 4.2, 20, 40, 60 and 100 K. All these spectra were fitted with a hyperfine field distribution and a doublet corresponding to a paramagnetic or superparamagnetic contribution. Relevant hyperfine parameters obtained from the fitting procedure are given in Table 2.

4. Discussion

$M(T)$ curves of sample S7 (see Fig. 3a)) show typical monodomain behavior with an T_{irr} of $T_{irr} > 300$ K. For $T > T_{irr}$, the $M(H)$ curves have a distinct measurement time, a shorter one, with respect to the $M(T)$ curves. In this way, they present a superparamagnetic behavior for $T \geq 250$ K and they are fitted with a Langevin function giving a monodomain magnetic moment $<\mu> = (3640 \pm 40)\ \mu_B$ at $T = 250$ K. For $T < T_{irr}$, the magnetization curves show irreversibility with square-like loops. Also the $H_C(T)$ shows monodomain behavior following a $T^{1/2}$ law. From the average magnetic moment, an estimated value of the diameter $<d> = 5.6$ nm was obtained, assuming spherical particles and a saturation magnetization of 80 emu/g (bulk value [22]). This diameter is slightly smaller than the one obtained by TEM. Taking the value of $<d>$ obtained from TEM analysis (7 nm) and using the Néel model $[\tau = \tau_0 \exp(K_{eff}V/k_BT]$ for the $M(T)$ measurements, assuming $\tau/\tau_0 = 10^{12}$ and $T = T_B$ to calculate the effective anisotropy constant (K_{eff}), the value of 2.0×10^6 erg/cm^3 is obtained, close to the values expected for Bulk material [22]. These conclusions are reinforced by MS analysis of this sample, where the in-field spectra can be easily related to the expected for monodomain nanoparticles, since they show the sextets that can be addressed to the contribution of Fe ions in the A and B sites of ferrite with an antiferromagnetic structure. The ratio of the absorption area between them indicates that the Co ions substitute the Fe ones preferentially in site B (octahedral). For this, the result obtained from Energy Disperse Spectroscopy (EDS) analysis (performed in a scanning electron microscopy-SEM) is compared with the Mössbauer one. From EDS analysis: at% Co/at% Fe = 0.38, while we observe a relation of the absorption intensity of site A/site B of about 0.7 in the MS for S7 sample at $H_{app} = 0$. For a perfect incorporation of Co ions in the site B, we expect a relation between the two absorptions about 0.85 (considering the amount of Co ions measured in the whole sample), and 0.45 for a random distribution of Co ions between A and B sites. Thus, about 85% of Co ions are in site B. In-field MS exhibit a partial alignments of the moments in sub-lattice A and B with applied field with lower values and an almost complete alignment for higher ones, despite a small

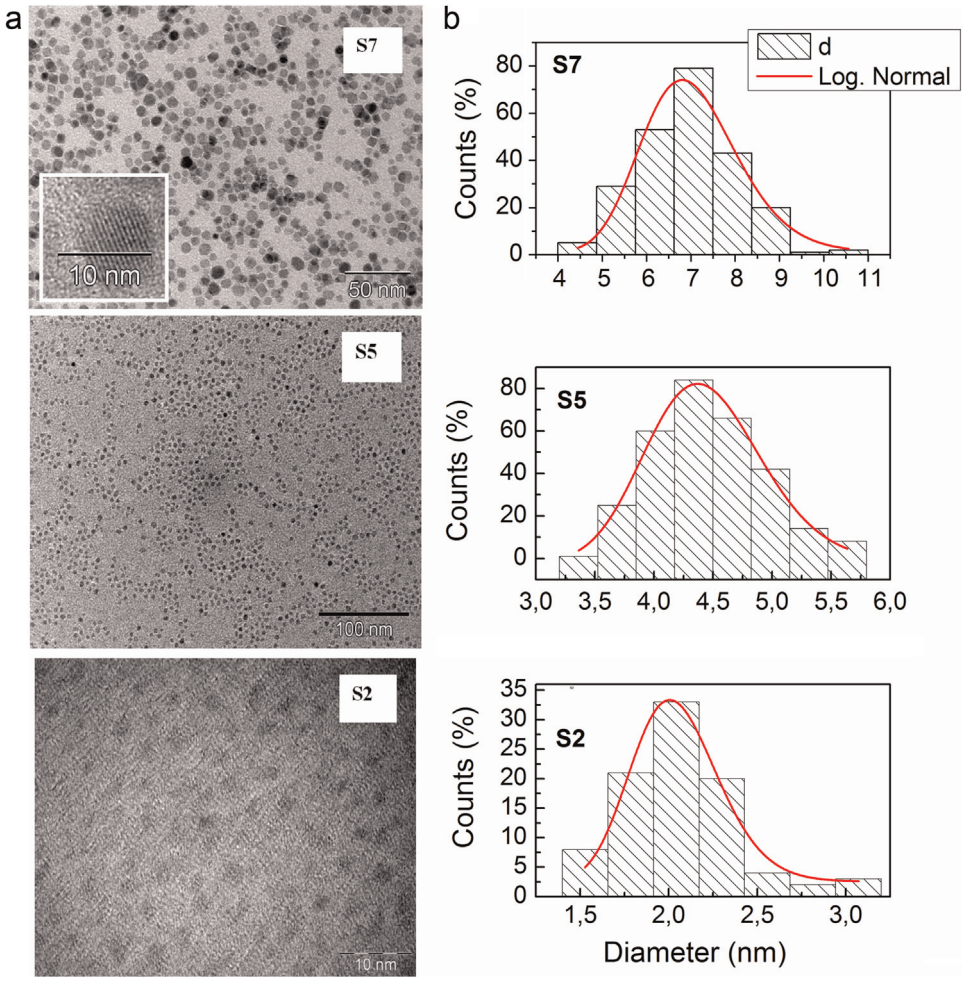

Fig. 2. Transmission electron microscopy (TEM) images of samples S7, S5 and S2. The right panel is the corresponding diameter histogram fitted with a log normal distribution, and the bottom inset is a high-resolution TEM image.

canting that are still observed at 120 kOe (a very small fraction, represented by the no null relation between the intensities of line 2 and line 3 (D_{23}) for both sites at 120 kOe).

$M(H)$ curves of S5 sample (see Fig. 4) exhibit two contributions to the magnetization for the entire range both in superparamagnetic and blocked regimes: a component that saturates at low magnetic fields, and a reversible component of the magnetization that does not saturate even for the maximum applied field of 50 kOe. In the superparamagnetic regime ($T > 170$ K) these curves are satisfactorily fitted by the equation $M(H,T)=M*(H,T)+\chi H$, where $M*$ has a superparamagnetic monodomain behavior described by an integral of Langevin functions [$L(x)=\coth(x)-1/x$, $x=\mu H/k_BT$] weighted by the lognormal particle size distribution and χH associated to the surface paramagnetic contribution. Another possibility is that the linear contribution at high field arises from small nanoparticles in superparamagnetic regime; however, TEM analysis did not indicate the presence of so small nanoparticles or a bimodal distribution. From these fitting the magnetic moment value of the single domain for each temperature was obtained. This value increases as the temperature decreases, as is shown in Fig. 8, indicating a progressive magnetic order inside the nanoparticle or, in other words, the growth of the single domain at lower temperatures. This magnetic fluctuation intra particle was also observed in NiAg heterogeneous alloys [23]. From a linear fit of the thermal dependence of the magnetic moment, we obtain the extrapolated magnetic moment for $T=0$, and from this value we estimated the value of the highly ordered monodomain diameter $<d>=4$ nm, close to the value obtained from TEM analysis. With this monodomain size and the average T_B a value of $K_{eff}=2.5\times10^6$ erg/cm^3 was determined by the Néel model, within the order of magnitude of the anisotropy constant calculated from the coercive field.

Below the T_{irr}, hysteresis curves are observed in the $M(H)$ plot as is usual for the blocked regime. The loops exhibit two contributions to the magnetization: a component that saturates at low fields, which is characteristic of the blocked single domain, and a reversible component of the magnetization that does not saturate even for the maximum applied field of 50 kOe. With decreasing temperature, H_C increases, following the usual $(1-(T/T_B)^{1/2})$ law for single domains, up to a maximum at $T_{H_C}^{max}=5$ K, as is showing in Fig. 5. Below this temperature, the coercive field decreases. The temperature of the maximum of $H_C(T)$ is the same temperature where the energy distribution $f(T)$ curve starts to grow as the temperature decreases. In Fig. 5, H_C vs $T^{1/2}$ is plotted evidencing only the typical monodomain behavior down to $T=5$ K, where the data exhibit a linear trend.

The simple model of a nanoparticle as a perfect ordered spin array, like in the bulk, is not valid to explain our results for sample S5, and the large disorder of the ferrimagnetic lattice due to the high surface to volume ratio should be considered. In fact, the

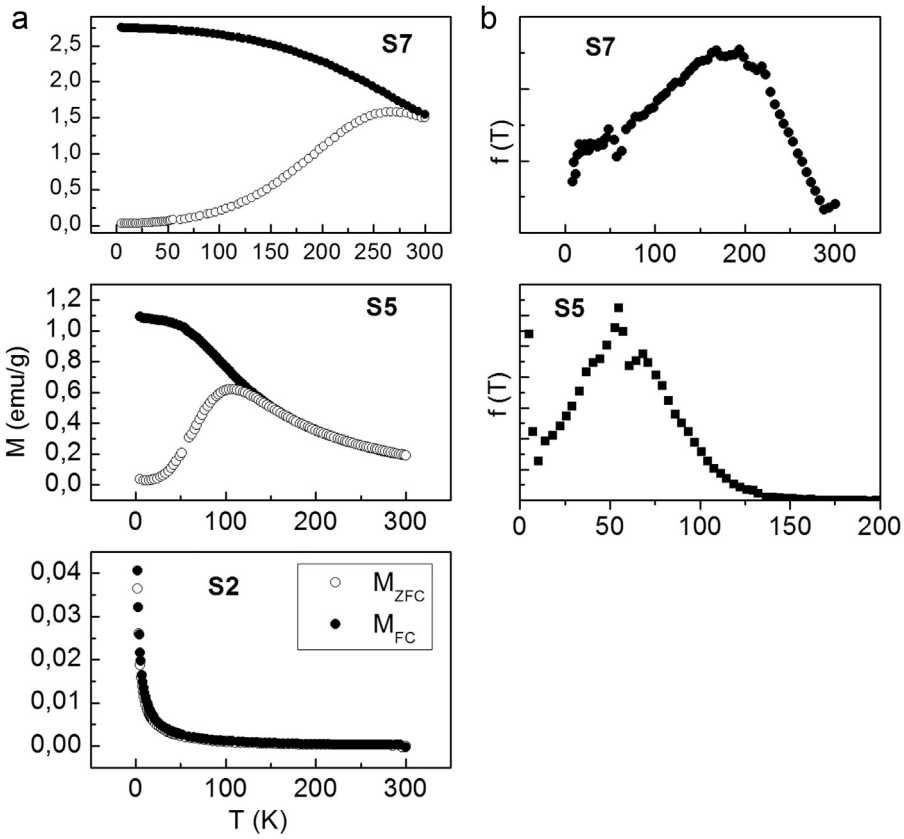

Fig. 3. (a) Magnetization curve as function of the temperature [$M(T)$] measured in ZFC and FC modes ($M_{ZFC}(T)$ and $M_{FC}(T)$) of samples S7, S5 and S2. (b) The blocking temperature distribution of samples S7 and S5 [calculated with Eq. (1)].

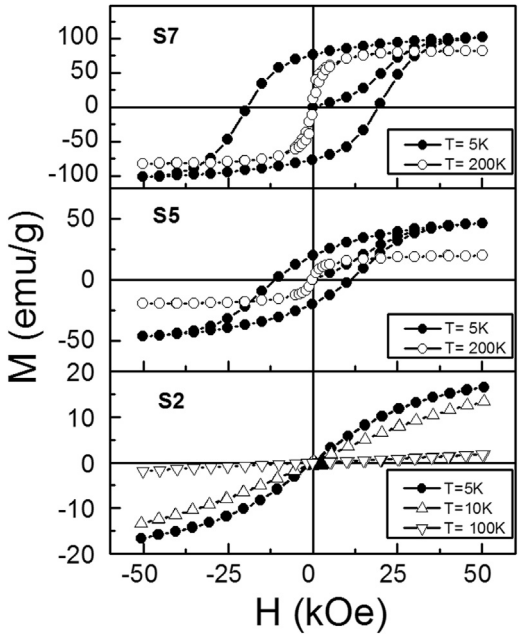

Fig. 4. Magnetization curve as function of the applied field [$M(H)$] measured in ZFC mode and different temperatures of samples S7, S5 and S2.

results for sample S5 can be satisfactorily interpreted by a core–shell model, which takes into account the competition between the surface anisotropy and the exchange interaction plus the crystalline anisotropy. In this case, the total energy per particle is given by [9,13,24,25]

$$E = -K_{core}(\mu_{core}\boldsymbol{z})^2 - \mu_{core}\boldsymbol{H} - \sum_{<i,\,a>}^{N_{shell}} J_{i,a}^{shell} S_i S_{i+a} - \sum_{i}^{N_{shell}} K_i^{shell}(S_i\boldsymbol{z})^2 - \sum_{i}^{N_{surf}} K_i^{surf}(\hat{S}_i\hat{\boldsymbol{n}}_i)^2 - \sum_{i}^{N_{shell}} \mu_i\boldsymbol{H} \quad (2)$$

where μ_{core} is the core magnetic moment, K_{core} and K_i are the crystalline anisotropy constant for the core and shell ions respectively, $J_{i,a}^{shell}$ is the exchange constant per ion between shell–shell ions and core spins–shell ions interaction (Co–Co, Fe–Fe or Co–Fe), K_i^{surf} is the surface anisotropy per atom (Fe or Co), i indicates a unit vector perpendicular to the surface, and $\hat{z}$ indicate the direction of the easy axis. The surface anisotropy term tends to align the spins perpendicular (parallel) to the surface for Fe (Co) magnetic moment, as reported in the literature [25]. It is clear that while the exchange interaction tends to magnetically order the system, the surface anisotropy favors its disorder. In the high-temperature regime, the surface spins are in a paramagnetic state, and we observe the superparamagnetic response of the ordered core plus the paramagnetic disordered shell. This disorder is originated by the competition between the exchange interaction and the crystalline anisotropy (which tend to magnetically order the particle), and the surface anisotropy, which depends on surface topology and tends to disorder the spins. Decreasing temperature, the ordered core volume increases and consequently the magnetic moment of the particle grows. Below $T=5$ K, the formation of surface spin clusters creates an additional effective field, and core moment-surface clusters moment interactions leading to the anomalous behaviors observed in the $H_C(T)$ and $M(T)$ curves [13,24,25].

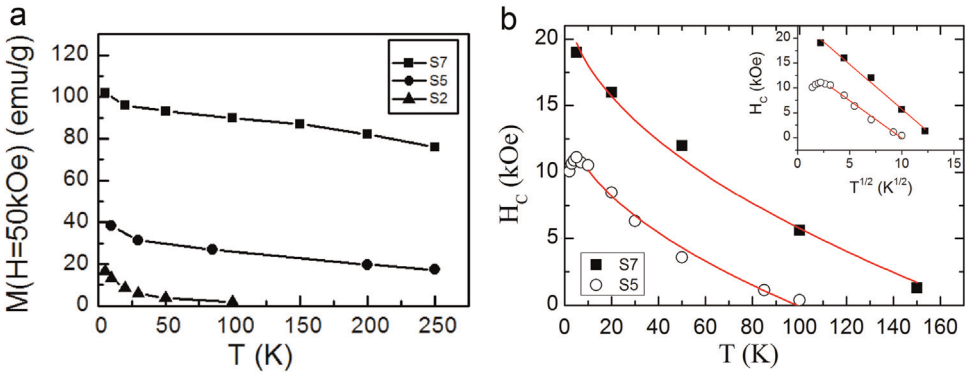

Fig. 5. (a) $M(T)$ curves measured with $H_{app}=50$ kOe of samples S7 and S5; (b) dependence of the coercive field with the temperature [$H_C(T)$] of samples S7 and S5, where the solid line correspond to the fit with $T^{1/2}$.

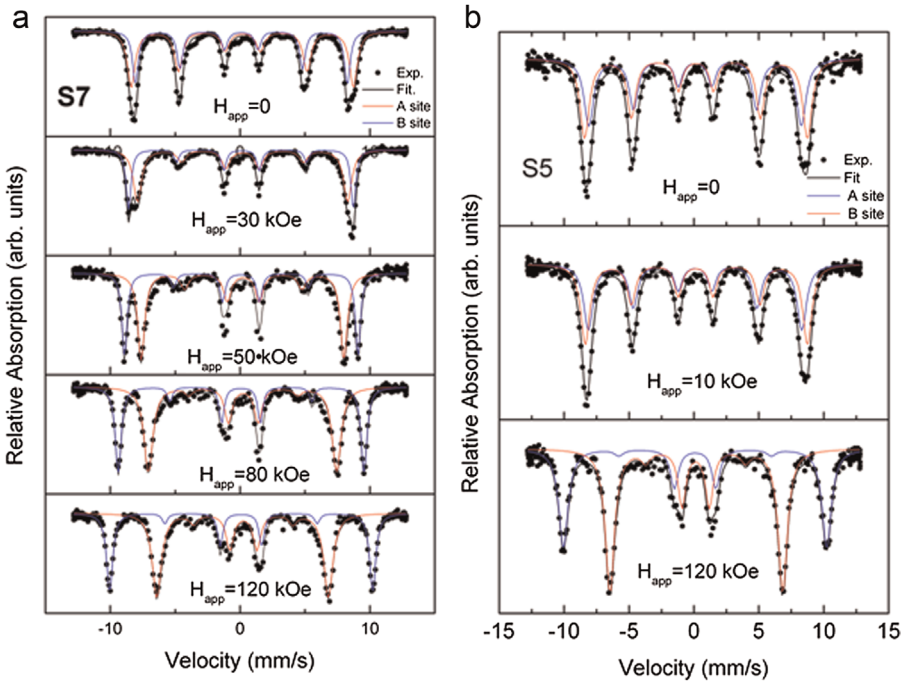

Fig. 6. (a) and (b) In-field Mössbauer spectra of samples S7 and S5, respectively, measured at 4.2 K. Each spectrum was fitted with two sextets referent to the contributions of sites A and B.

Table 1
Relevant hyperfine parameters obtained from the fitting procedure of Mössbauer spectra of samples S7 and S5 at 4.2 K. B_{eff} is the effective field, IS is the Isomer Shift, QS is the Quadrupolar Spliting and D23 is the ratio between the intensities of lines 2 and 3 of the sextet.

Sample	μH_{app} (T)	Crystalline site	B_{eff} (T)	IS (mm/s)	QS (mm/s)	D23	Absorption area (%)
S7	0	A	50.90	0.26	0.01	2.00	41
		B	53.30	0.36	−0.04	2.00	59
	3	A	53.80	0.27	0.01	0.60	41
		B	50.30	0.37	−0.04	0.66	59
	5	A	55.85	0.26	0.01	0.51	41
		B	48.52	0.40	−0.06	0.55	59
	8	A	58.79	0.25	0.01	0.40	41
		B	45.04	0.40	−0.06	0.20	59
	12	A	62.94	0.26	0.01	0.31	41
		B	41.04	0.40	−0.06	0.28	59
S5	0	A	50.80	0.27	0	2.1	47
		B	53.30	0.34	0.05	2.0	53
	1	A	51.10	0.27	0	1.5	47
		B	53.20	0.34	0.05	1.4	53
	12	A	62.90	0.27	0	0.17	41
		B	41.40	0.34	0.05	0.23	59

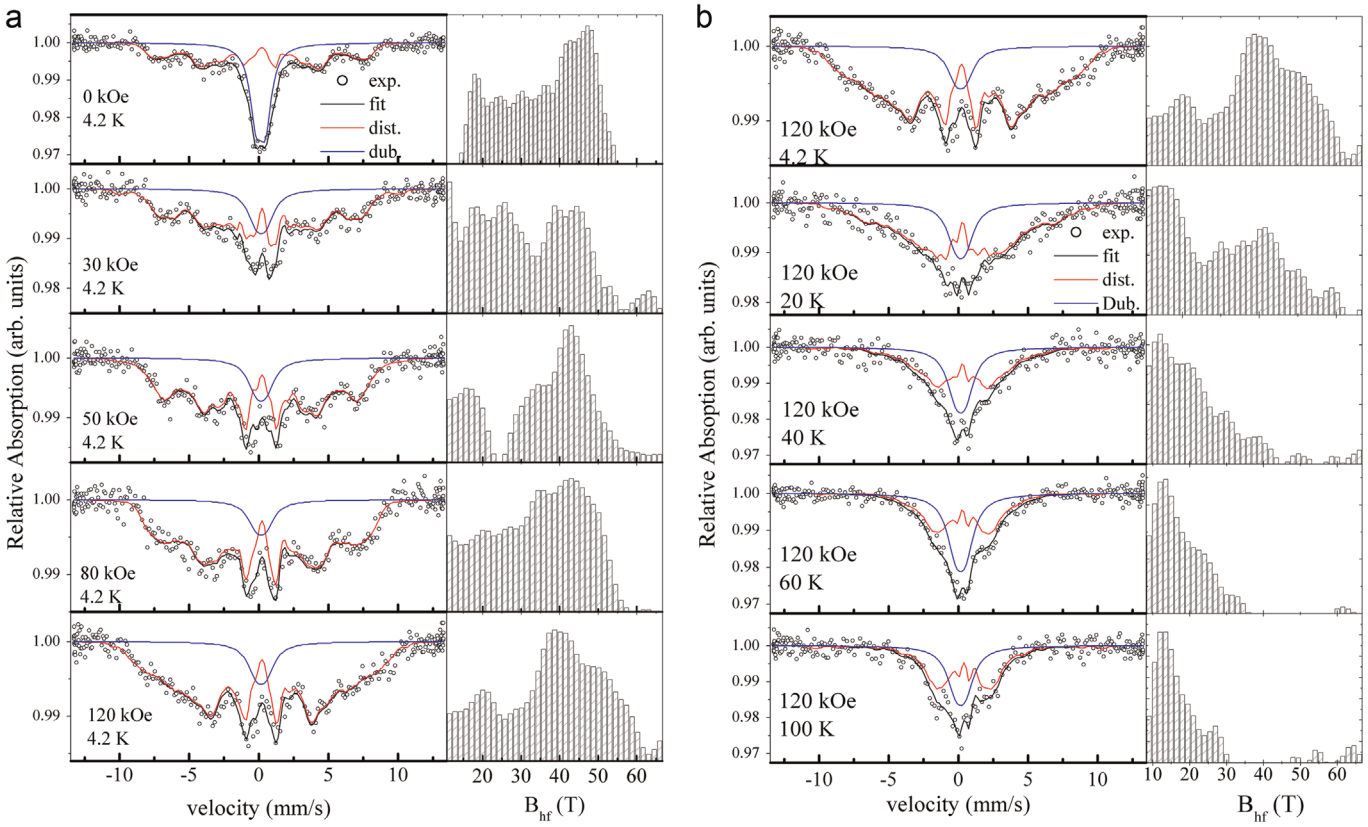

Fig. 7. (a) In-field Mössbauer spectra of sample S2 measured at 4.2 K; (b) in-field Mössbauer spectra measured with $H_{app}=120$ kOe at different temperatures. The right panel shows the respective hyperfine field distribution.

Interestingly, the in-field MS of sample S5 are also composed of the contribution of the two sextets (sites A and B). For this sample, we can estimate that about 90% of Co ions are in site B. If we focus at lower field (10 kOe), we observe a large value for D_{23} for both A and B sites for sample S2 in comparison to sample S7. These Mössbauer results indicates a larger canting for a larger number of moments in sample S5 in comparison with sample S7 for both sites, despite they are present for a small number of spins considering the whole sample and it is more significant for site B. The mean value of the canting angle ($<\beta>$ = mean angle between H_{app} and the magnetic moment) is given by

$$\sin^2\langle\beta\rangle = \frac{2D_{23}}{4 + D_{23}} \tag{3}$$

Our magnetization results at high fields for Sample S5 indicates that the value of D_{23} observed in the MS comes from a fraction of magnetic moments in both sites misaligned with respect to H_{app}. In this case, these moments also leads to a change in the values of the B_{hf} in comparison with the corresponding core sub-spectrum; however, because of the broad peaks and the small changes expected in the B_{hf} (because of the values of D_{23}, indicating a partial

Table 2
Hyperfine parameters obtained from the fitting procedure of the in-field Mössbauer spectra of sample S2: B_{hf} (most probable hyperfine fields), w (half width at half height), IS (isomer shift), QS (quadrupolar splitting), D23 (relation between the absorption area of lines 1 and 3).

Applied field (kOe)	T (K)	Subspectra	B_{hf} (T)	IS (mm/s)	QS (mm/s)	W (mm/s)	D23	Absorption area (%)
0	4.2	Distribution	43.4 /47.3	0.25/0.41	−0.01	–	2	55
		Doublet	–	0.35	0.7	1.1	–	45
30	4.2	Distribution	44.3 / 38.5	0.25/0.41	−0.01	–	1.5	72
		Doublet	–	0.35	0.7	1.3	–	28
50	4.2	Distribution	42.9 / 35.9	0.25/0.41	−0.01	–	1.5	90
		Doublet	–	0.35	0.7	1.3	–	10
80	4.2	Distribution	48.7 / 43.5 / 35.6	0.25/0.30/0.41	−0.01	–	1.3	90
		Doublet	–	0.35	0.7	1.3	–	10
120	4.2	Distribution	49.8 / 39.4	0.25/0.41	−0.01	–	1.4	90
		Doublet	–	0.35	0.7	1.3	–	10
120	20	Distribution	14.5	0.35	−0.01	–	2	88
		Doublet	–	0.35	0.7	1.3	–	12
120	40	Distribution	12.6	0.35	−0.01	–	2	61
		Doublet	–	0.35	0.7	1.1	–	39
120	60	Distribution	13.6	0.35	−0.01	–	2	52
		Doublet	–	0.35	0.7	1.1	–	48
120	100	Distribution	12.6	0.35	−0.01	–	2	50
		Doublet	–	0.35	0.7	1.3	–	50

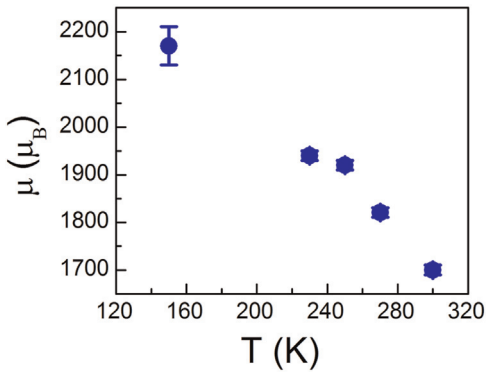

Fig. 8. Magnetic moment of sample S5 obtained from the fitting of $M(H)$ curve with the Langevin equation plus a linear contribution as function of the temperature.

misalignment), the contribution of the misaligned magnetic moments is not observed as separated sextets.

The magnetic behavior of the sample S2 is compatible with a paramagnetic sample (or not fully magnetically ordered one). In fact, the calculated mean magnetic moment of the nanoparticles of this sample from the $M(H)$ curves is $\mu(T=5\,K)=(4.92\pm0.02)\mu_B$. This result give us the evidence that the poor crystallinity of these nanoparticles and the large surface/volume ratio avoid the ferrimagnetic order in the particle down to $T=5$ K. Some irreversibility in $M(T)$ curves is observed, but it can be easily addressed to the a small amount of larger particles (>3 nm) observed for this sample in TEM images. However, $M(H)$ measurements clearly reinforces the lack of magnetic order in this sample.

In-field MS of sample S2 at low temperature (4.2 K) were fitted with a distribution of hyperfine fields and a doublet, which corresponds to a superparamagnetic or paramagnetic contribution, and the obtained fit confirms the analysis from magnetization measurements. Despite the fact that the hyperfine field distributions present two maxima, which can be associated to sites A and B, the variation of these values with H_{app}, as well as the variation of D23, it is not the expected for two sub-lattice with antiferromagnetic alignment in parallel direction with respect to the applied field. The values of B_{hf} observed for these two maxima are smaller than the expected for sites A and B in the ferrite. In addition, we observe an important contribution in low values of B_{hf}, which may correspond to relaxation phenomena, spins with relaxation time close to the time window of the experiment (10^{-8} s). This contribution at low values of B_{hf} decreases with increasing H_{app}, indicating some ordering process with the increment of the external field. The doublet indicates a superparamagnetic or paramagnetic contribution [26–28] even at 4.2 K. Its relative absorption area decreases, while w slightly increases, with increasing external field, also indicating the increment in the magnetic order with H_{app}. Therefore, in-field MS at 4.2 K indicates a lack of the antiferromagnetic order in sample S2, in accordance with the magnetization measurements. In-field MS spectra with $H_{app}=120$ kOe and $T=4.2$, 20, 40, 60 and 100 K shows an increment in the relative absorption area of the doublet with increasing T, as expected for a paramagnetic or superparamagnetic contribution. At the same time, the distribution strongly dislocates for low values of B_{hf}, which is also expected as consequence of the increment of the relaxation phenomena with increasing temperature.

5. Conclusions

We have synthesized $CoFe_2O_4$ nanoparticles with sizes in the 2–7 nm range in order to study the influence of the surface anisotropy in the internal magnetic order of the particles. Particles with $d=7$ nm have almost single-domain behavior and the monodomain occupies approximately the whole particle. In the sample with $d=5$ nm, the surface anisotropy is large enough to alter the ferrimagnetic order in the particle shell. Then, a surface/volume ratio of $\sim$60% is the crossover between a single domain nanoparticle and a frustrated order in a magnetic core–shell structure, due to the competition between surface anisotropy and exchange interaction+crystalline anisotropy in cobalt ferrite. In the sample with $d=2$ nm, the poor crystallinity and the large surface/volume ratio avoid the ferrimagnetic order in the particle down to $T=5$ K.

Acknowledgments

This work was supported by Argentinean grants PIP 1333/08 (CONICET), PICT 0832/07 and Universidad Nacional de Cuyo 06-C404, as well as by the Brazilian agency FAPESP (Proc: 2011/50556-0).

References

[1] R.H. Kodama, A.E. Berkovitz, E.J. Mc Niff Jr, S. Foner, Phys. Rev. Lett. 77 (1996) 394.
[2] O. Iglesias, A. Labarta, Phys. Rev. B 63 (2001) 1844416.
[3] Fiorani, D. (Ed.), 2005. Surface Effects in Magnetic Nanoparticles, Springer. ISBN 0-387-23279-6.
[4] J.M.D. Coey, Phys. Rev. Lett 27 (1971) 1140.
[5] R.H. Kodama, A. Salah, A. Makhlouf, A.E. Berkovitz, Phys. Rev. Lett. 79 (1997) 1393.
[6] H. Kachkachi, A. Ezzir, M. Noguès, E. Tronc, Eur. Phys. J. B 14 (2000) 681.
[7] N. Pérez, P. Guardia, A.G. Roca, M.P. Morales, C.J. Serna, O. Iglesias, F. Bartolomé, L.M. García, X. Batlle, A. Labarta, Nanotechnology 19 (2008) 475704.
[8] J.M. Vargas, E. Lima Jr., R.D. Zysler, J.G. Santos Duque, E. De Biasi, M. Knobel, Eur. Phys. J. B 64 (2008) 211.
[9] E. Winkler, R.D. Zysler, M. Vasquez Mansilla, D. Fiorani, Phys. Rev. B 72 (2005) 132409.
[10] E. Winkler, R.D. Zysler, D. Fiorani, Phys. Rev. B 70 (2004) 174406.
[11] E. Lima Jr., E. De Biasi, M. Vasquez Mansilla, M.E. Saleta, F. Effenberg, L.M. Rossi, R. Cohen, H.R. Rechenberg, R.D. Zysler, J. Appl. Phys. 108 (2010) 103919.
[12] P. Dutta, A. Manivannan, M.S. Seehra, N. Shah, G.P. Huffman, Phys. Rev. B 70 (2004) 174428.
[13] E. De Biasi, C.A. Ramos, R.D. Zysler, H. Romero, Phys. Rev. B 65 (2002) 144416.
[14] José M. Vargas, Roberto D. Zysler, Nanotechnology 16 (2005) 1474.
[15] C. Vázquez-Vázquez, M.A. López-Quintela, M.C. Buján-Núñez, J. Rivas, J. Nanopart. Res. 13 (2011) 1663.
[16] I. Sharifi, H. Shokrollahi, M.M. Doroodmand, R. Safi, J. Magn. Magn. Mater 324 (2012) 1854.
[17] B. Bittova, J. Poltierova Vejpravova, M.P. Morales, A.G. Roca, A. Mantlikova, J. Magn. Magn. Mater. 324 (2012) 1182.
[18] Kai Zhang, T. Holloway, A.K. Pradhan, J. Magn. Magn. Mater. 323 (2011) 1616.
[19] B.D. Cullity, S.R. Stock, Elements of X-Ray diffraction, 3rd ed., Prentice-Hall Inc. (2001) 167–176.
[20] M. Knobel, L.M. Socolovsky, J.M. Vargas, Rev. Mex. Fís. 50 (2004) 8–28.
[21] M.G.M. Miranda, G.J. Bracho Rodríguez, A.B. Antunes, M.N. Baibich, E.F. Ferrari, F.C.S. da Silva, M. Knobel, J. Magn. Magn. Mater. 185 (1998) 331–338.
[22] R.C.O. Handley, Modern Magnetic Materials: Principles and Applications, Wiley & Sons, 1999 (Chapter 10).
[23] L.C.C.M. Nagamine, B. Mevel, B. Dieny, B. Rodmacq, J.R. Regnard, C. Revenant-Brizard, I. Manzini, J. Magn. Magn. Mater. 195 (1999) 437–451.
[24] R.D. Zysler, H. Romero, C.A. Ramos, E. De Biasi, D. Fiorani, J. Magn. Magn. Mater. 266 (2003) 233.
[25] E. De Biasi, C.A. Ramos, R.D. Zysler, H. Romero, D. Fiorani, Phys. Rev. B 71 (2005) 104408.
[26] S. Mørup, J. Magn. Magn. Mater. 37 (1983) 39.
[27] M.S. Kamali-, T. Ericsson, R. Wäppling., Thin Solid Films 515 (2006) 721.
[28] L. Häggström, S. Kamali, T. Ericsson, P. Nordblad, A. Ahniyaz, L. Bergström, Hyperfine Interact. 183 (2008) 49.